UNIVERSITAT DE BARCELONA

Departament d'Astronomia i Meteorologia

Astrophysical Studies on Open Clusters:

NGC 1807, NGC 1817, NGC 2548 and NGC 2682

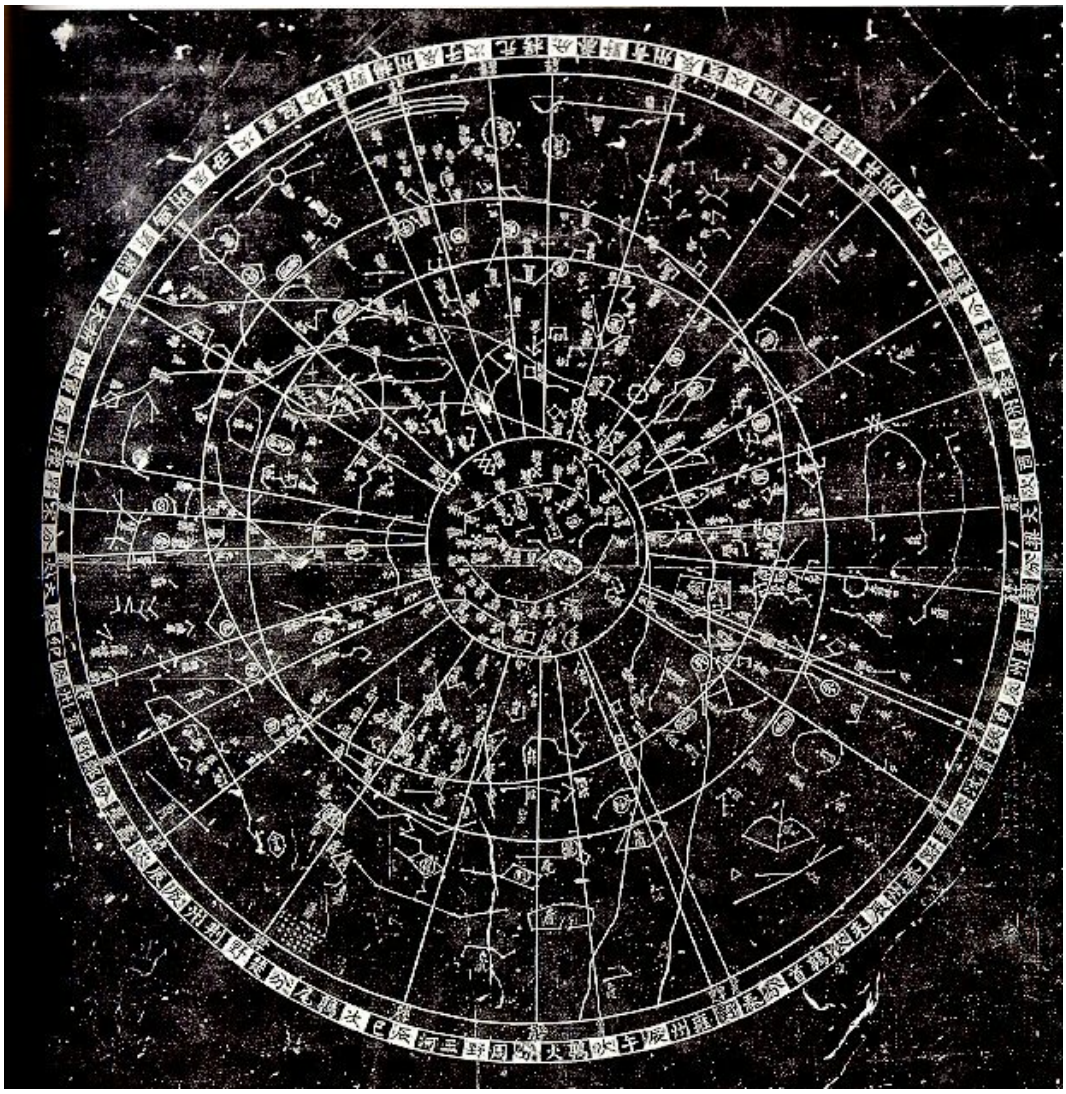

Memoria presentada por

María de los Dolores Balaguer Núñez

para optar al grado de

Doctora en Física

Barcelona, 31 de octubre de 2005

中秋月

暮云收尽溢清寒
银汉无声转玉盘
此生此夜不长好
明年明月何处看

苏轼 (1036-1101)

Mid-Autumn Moon

The sunset clouds are gathered far away, it is clear and cold,
The Milky Way is silent, I turn to the jade plate.
The goodness of this life and of this night will not last for long,
Next year where will I watch the bright moon?

Su Shi (1036 - 1101)

4 NGC 2548 (M 48): Proper motions and membership probabilities

Proper motions of bright stars in the region of NGC 2548 were first published by Ebbighausen (1939) from four pairs of plates and a maximum epoch difference of only 28 years. Li (1954) published positions and proper motions in the field of NGC 2548 based on three plates taken with the 40 cm astrograph at Shanghai Zǒ-Sè station with a maximum epoch difference of only 14 years. It has not been the object of any recent complete astrometric study.

In this Chapter[1], we determine, for the first time, precise absolute proper motions of 501 stars within a 1.°6× 1.°6 area in the NGC 2548 region, from automatic MAMA[2] measurements of 10 plates. Five of them were newly taken in 1998, resulting in an epoch difference of 82 years. The estimated membership probabilities combining parametric and non-parametric methods led us to a complete astrometric study of the cluster area.

[1]This Chapter is based on: Wu Z.Y., Tian K.P., Balaguer-Núñez L., Jordi C., Zhao J.L., & Guibert J., 2002, A&A 381, 464 and Balaguer-Núñez L., Jordi C., & Galadí-Enríquez D., 2005, A&A 437, 457

[2]MAMA (Machine Automatique à Mesurer pour l'Astronomie, `http://dsmama.obspm.fr`) is developed and operated by INSU/CNRS and Observatoire de Paris.

Table 4.1: Plate material of NGC 2548 area

Plate Id.	Epoch (1900+)	Exp.Time min	Plate centre (α_{J2000} δ_{J2000})	Plate size cm	n. of stars
CL422	16.03.24	90	$8^h.2283$ $-5°.779$	24×30	450
CL534	30.03.21	90	$8^h.2286$ $-5°.775$	24×30	556
CL535	30.03.28	90	$8^h.2291$ $-5°.767$	24×30	566
CL56006	56.03.14	60	$8^h.2288$ $-5°.779$	24×30	577
CL56007	56.03.16	60	$8^h.2372$ $-5°.779$	24×30	558
CL98004	98.04.03	30	$8^h.2447$ $-5°.958$	24×30	548
CL98047	98.12.16	30	$8^h.2227$ $-5°.796$	20×20	268
CL98Tian	98.12.25	30	$8^h.2255$ $-5°.804$	20×20	268
CL98Chen	98.12.25	30	$8^h.2255$ $-5°.804$	20×20	298
CL98Gu	98.12.16	30	$8^h.2227$ $-5°.796$	20×20	432

4.1 Plate measurement and proper motion reduction

4.1.1 Plate material and measurements

Ten plates of the NGC 2548 region were available (five were old ones, and the other five were exposed for this work). As in the case of NGC 1817, all were taken with the double astrograph at the Zô-Sè station of Shanghai Observatory. The size of the old plates is 24 cm by 30 cm, or $2°.0 \times 2°.5$, and that of the new ones is 20 cm by 20 cm, or $1°.65 \times 1°.65$. The oldest plate was taken in 1916, and the newest ones in 1998. Relevant information on these plates is shown in Table 4.1.

All plates were measured at the Centre d'Analyse des Images at the Observatoire de Paris, using the high precision microdensitometer "Machine Automatique à Mesurer pour l'Astronomie" (MAMA). This device has a superb optical and mechanical performance (Guibert et al. 1990). It uses a quartz-iodine illuminating source, whose transmitted light is detected by a reticon, 1024 pixels large, with a pixel size of 10 μm, and the absolute accuracy of the measurements is 0.6 μm (Soubiran 1992). After the plates were scanned, the resulting images were stored in a grid

of 19 × 19 sub-images for each plate. Once every plate was digitised, we identified all point sources in these 361 frames. The source extraction was performed on each frame using SExtractor (Bertin & Arnouts 1996), a software dedicated to the automatic analysis of astronomical images using a multi-threshold algorithm allowing good object deblending. To improve the accuracy of the measurements, we chose to retain only rather bright objects with a signal-to-noise ratio of at least 12.

During the scanning, MAMA includes in the catalogue not only real images, but also the plate grid (if present), emulsion flaws, plate annotations and scratches. A first step is required to reject spurious detections, most of which can be recognised with the analysis of the object shape, by removing the plate grid, annotations and big scratches by visual comparison with the original plates. The shape parameters given by SExtractor can be used to clarify the remaining stars but the most direct way to reject spurious detection is by comparison between plates, searching each object from one plate to the other, and retaining only the paired data. There is a total of 596 stars measured with a limiting magnitude $B_{\rm T}$ around 14. This limiting magnitude was roughly estimated from the stars in common with Tycho-2 Catalogue (Høg et al. 2000).

The detection of 182 PPM (Röser & Bastian 1991) and ACT (Urban et al. 1997) stars on the whole plate allowed us to determine the star positions in a common system. Thus for each scanned plate, we obtained a preliminary astrometric catalogue to perform initial cross-identification between plates.

4.1.2 Absolute proper motions

The absolute proper motions for 596 stars in the region of NGC 2548 were reduced on the basis of the MAMA measurements following the central overlapping procedure (Russel 1976; Wang et al. 1995, 1996, 2000). The data treatment was the same as described in Section 2.5. Stellar positions and absolute proper motions were reduced from a catalogue used as the original data for the first iteration. As initial catalogue, 265 stars from the Tycho-2 Catalogue at epoch J2000 (Høg et al. 2000) were chosen on the basis of the results of the PPM and ACT astrometric catalogue given by MAMA. To select the best plate constant model, we used Eichhorn & Williams' criterion (Eichhorn & Williams 1963, Wang et al. 1982) and obtained a model with six linear constants on coordinates, a magnitude and a coma term,

Table 4.2: Mean precisions of proper motions as a function of the number of plates in the NGC 2548 region. (Units are mas yr^{-1}.) Columns "N. plates" and "N" give the number of plates and stars, respectively.

N. plates	N	$\epsilon_{\mu_\alpha \cos\delta}$	ϵ_{μ_δ}	ϵ_μ
3	4	5.29	2.90	6.30
4	8	2.92	3.12	4.44
5	46	1.76	1.11	2.19
6	119	1.19	0.89	1.53
7	27	1.15	0.76	1.42
8	20	0.90	0.70	1.17
9	50	0.74	0.55	0.94
10	199	0.59	0.46	0.77

and a magnitude distortion term (Equations 2.12 and 2.13). Magnitudes used were the instrumental magnitudes. All the proper motions are constrained by having at least one measurement from the modern epoch plates, i.e. taken in 1998. The whole process is iterated until the resulting proper motions converge. We iterate the process until mean differences in position are smaller than 1.1 mas, the r.m.s. smaller than 3.6 mas and the differences in proper motion below 0.1 mas yr^{-1}, yielding a final outcome of 501 stars.

Table 4.2 shows mean precisions of final proper motions detected on different numbers of measured plates (greater than 2). The precision of the final proper motions strongly depends on the number of plates. Figure 4.1 gives the number of stars for which various numbers of plates are available. More than 90% of proper motions were obtained from at least 5 plates.

The mean errors of proper motions for more than 90% of stars are $\epsilon_{\mu_\alpha \cos\delta}$= 0.92 mas yr^{-1}, ϵ_{μ_δ} = 0.68 mas yr^{-1} and ϵ_μ= 1.18 mas yr^{-1}, where $\epsilon_\mu = \sqrt{\epsilon^2_{\mu_\alpha \cos\delta} + \epsilon^2_{\mu_\delta}}$. In the most precise case, the errors are 0.77 mas yr^{-1} for stars with 10 plates (40% of stars). Figure 4.2 shows the distribution of proper motion errors with the number of stars: N versus $\epsilon_{\mu_\alpha \cos\delta}$, ϵ_{μ_δ} and ϵ_μ. The better quality of these results compared to those of the similar study of NGC 1817 in Chapter 2 can be attributed to the excellent positioning behaviour of the MAMA scanning machine.

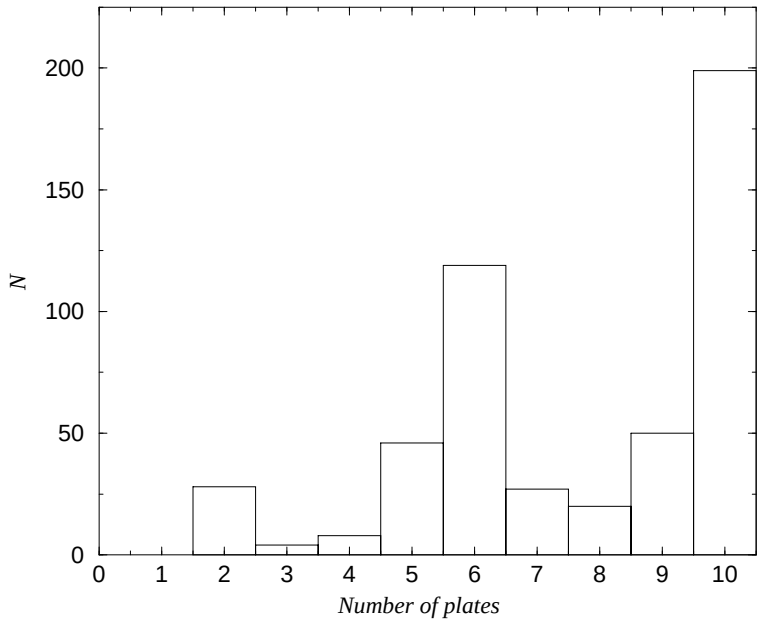

Figure 4.1: The number of stars vs the number of available plates

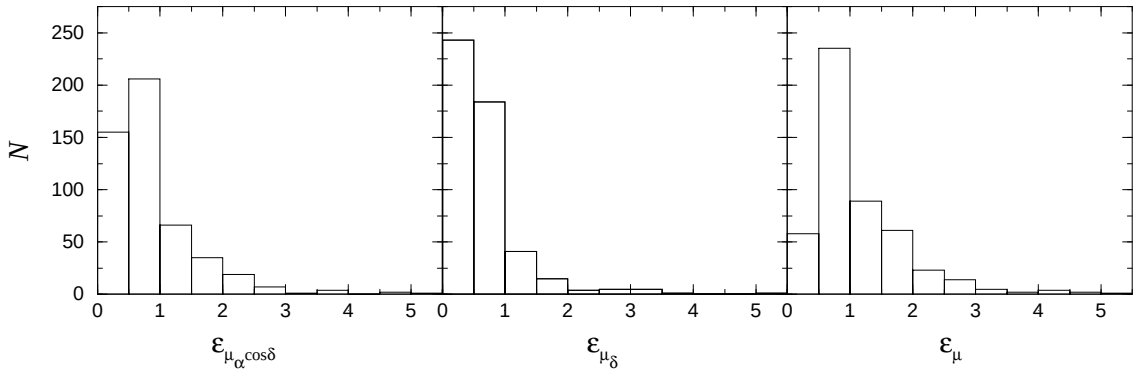

Figure 4.2: The number of stars vs the errors in proper motions (units are in mas yr^{-1})

Figure 4.3 gives $\mu_\alpha \cos\delta$, μ_δ and their errors with respect to instrumental magnitude.

Our absolute proper motions and their errors are compared with those of Tycho-2 Catalogue in Figure 4.4. Mean differences in the sense ours minus Tycho-2 are -0.123 ($\sigma = 2.112$) mas yr^{-1} and -0.203 ($\sigma = 2.158$) mas yr^{-1} in $\mu_\alpha \cos\delta$ and μ_δ, respectively. No apparent systematic residuals were found as a function of magnitude. A linear fit to the proper motion data gives us:

$$\mu_\alpha \cos\delta = 0.187\ (\pm 0.133) + 0.982\ (\pm 0.009) \cdot (\mu_\alpha \cos\delta)_{\rm Tyc2}\ ;\ r = 0.988$$

$$\mu_\delta = 0.201\ (\pm 0.132) + 1.016\ (\pm 0.008) \cdot (\mu_\delta)_{\rm Tyc2}\ ;\ r = 0.992$$

being r the correlation coeficient.

Only 8 stars were found in this region from the Hipparcos Catalogue (ESA 1997). By comparing absolute proper motions for these common stars, the mean differences are (in the sense ours minus Hipparcos) -0.610 ($\sigma = 1.710$) mas yr^{-1} and -0.198 ($\sigma = 1.658$) mas yr^{-1} in $\mu_\alpha \cos\delta$ and μ_δ, respectively. We obtain the following linear fit:

$$\mu_\alpha \cos\delta = -0.458\ (\pm 0.756) + 1.005\ (\pm 0.013) \cdot (\mu_\alpha \cos\delta)_{\rm HIP}\ ;\ r = 0.999$$

$$\mu_\delta = -0.470\ (\pm 0.694) + 1.011\ (\pm 0.014) \cdot (\mu_\delta)_{\rm HIP}\ ;\ r = 0.999$$

4.2 Membership determination

NGC 2548 is a very extended object with a complex structure with a double core, prolate shape and a possible tidal tail with a clump (Bergond et al. 2001). It has been suggested that the nature of this secondary clump is associated with the last strong disk shock which occurred between 20 and 40 Myr ago. Confirmation of members at large radii would trace the distribution of stars which are currently leaving the cluster. This could help to constrain models of the tidal disruption of open clusters, a topic of considerable current observational and theoretical interest. As in Chapter 2, we compare and combine the parametric and non-parametric approach to the cluster/field segregation.

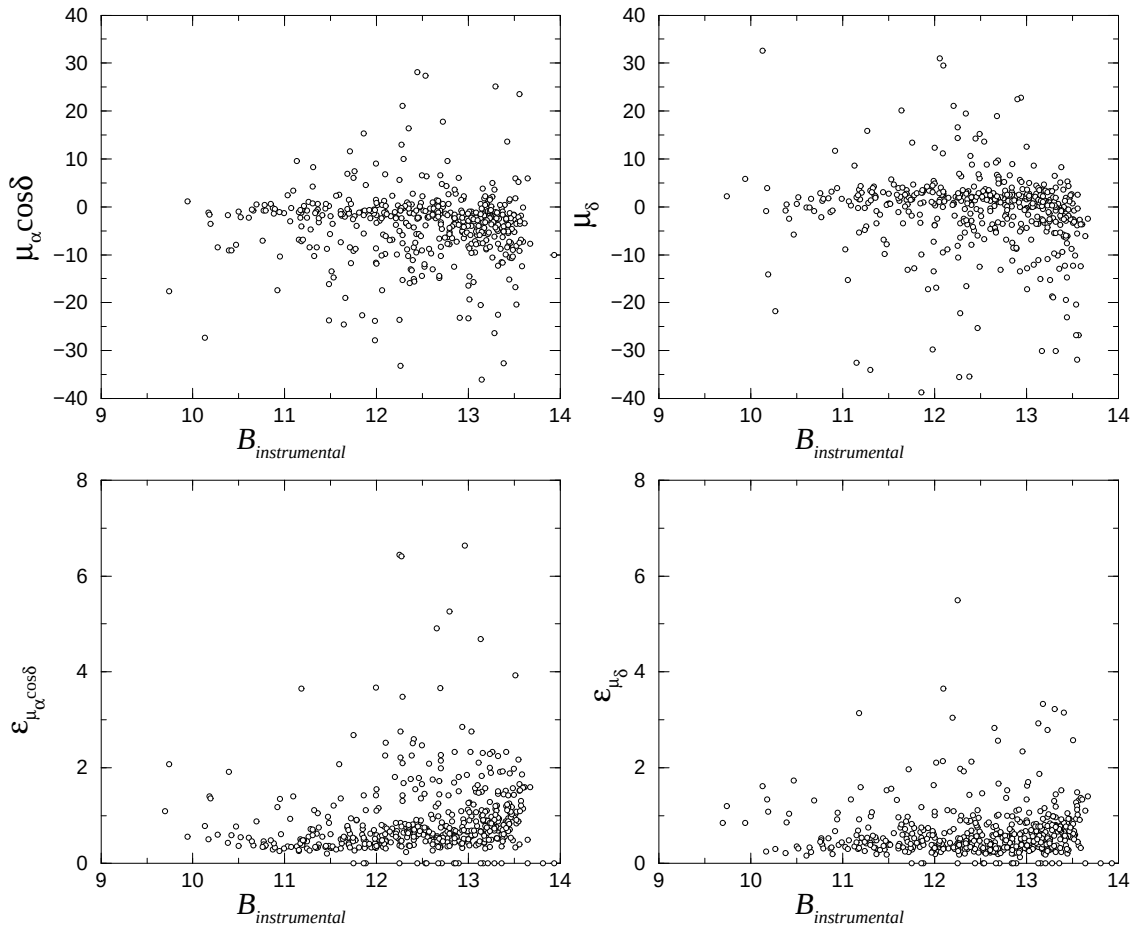

Figure 4.3: Proper motions (top) and their errors (bottom) vs instrumental magnitude. Null errors are from proper motions calculated with only two plates. (Units are mas yr^{-1})

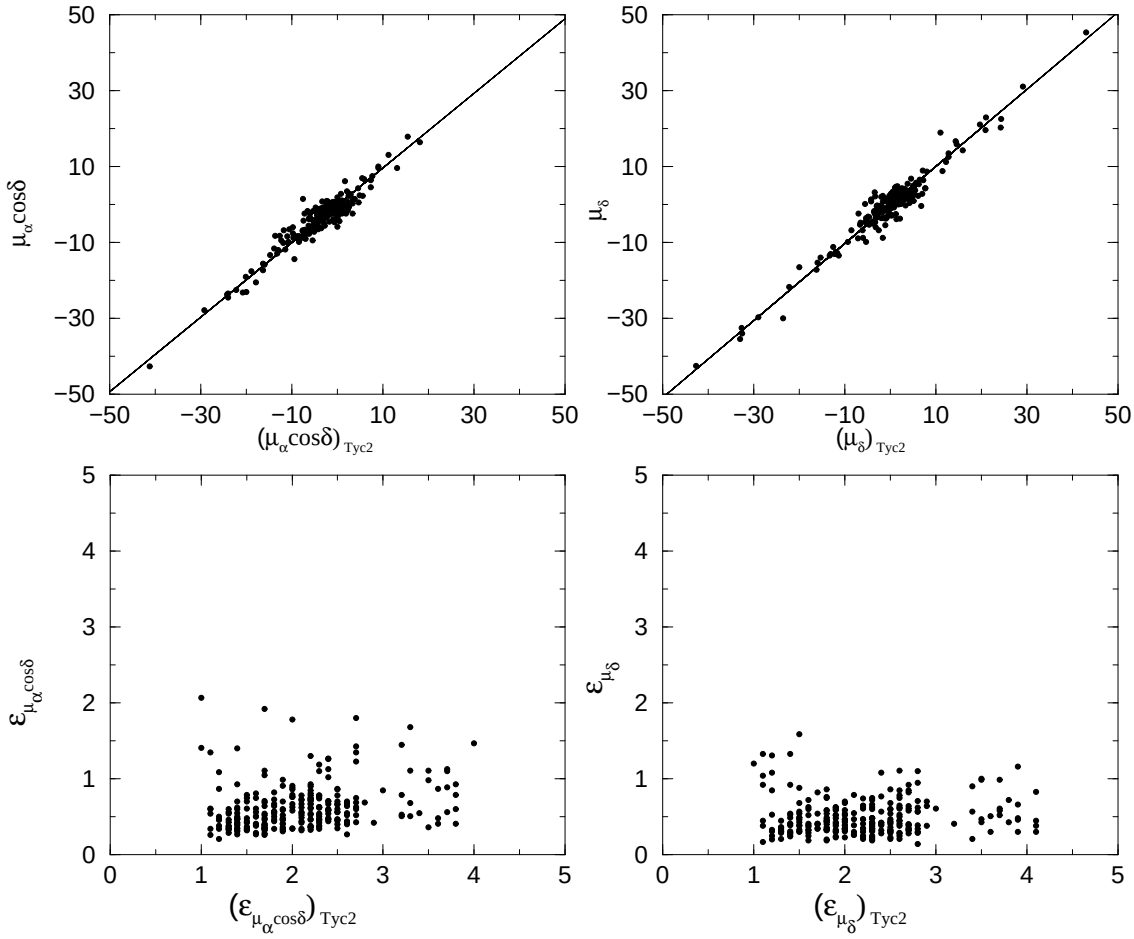

Figure 4.4: Proper motions and their errors from this study compared to those in Tycho-2 Catalogue. (Units are mas yr^{-1})

Table 4.3: Distribution parameters and their uncertainties for NGC 2548. The units of μ and σ are mas yr^{-1}.

	n_c	$\mu_\alpha \cos\delta$	μ_δ	σ_c	$\sigma_{\mu_\alpha \cos\delta}$	σ_{μ_δ}	ρ
NGC 2548	0.382	−1.41	1.64	1.23			
	±0.025	±0.12	±0.12	±0.08			
field		−4.89	−1.63		7.37	8.21	−0.28
		±0.07	±0.57		±0.04	±0.29	±0.03

4.2.1 The classical approach

We used a maximum likelihood method with a 9-parametric Gaussian model for the frequency function, as in Section 2.6.1. The unknown parameters for the assumed Φ distribution are $[n_c,\ (\mu_\alpha \cos\delta)_c,\ (\mu_\delta)_c,\ \sigma_c]$ for the cluster and $[(\mu_\alpha \cos\delta)_f,\ (\mu_\delta)_f,\ \sigma_{(\mu_\alpha \cos\delta)_f},\ \sigma_{(\mu_\delta)_f},\ \rho]$ for the field population.

By applying the standard maximum likelihood method, we obtained the 9 distribution parameters and their corresponding uncertainties, shown in Table 4.3. The quality of the fit should be optimised near the proper motion region occupied by the cluster stars, where the model is most crucial to providing reliable membership determination. To minimise the effect of high proper-motion field stars in the model, we restricted the membership determination to the range $|\mu| < 30$ mas yr^{-1}.

Table 4.4[3] lists the results for all 501 stars in the region of the open cluster: column 1 is the ordinal star number; columns 2 and 3 are $\alpha_{\rm J2000}$ and $\delta_{\rm J2000}$; columns 4 and 6 are the respective absolute proper motions $(\mu_\alpha \cos\delta, \mu_\delta)$; columns 5 and 7 are the standard errors of the proper motions; column 8 is the parametric membership probability of stars belonging to NGC 2548 (P_P); column 9 is the instrumental magnitude given by SExtractor; column 10 gives the number of plates used and column 11 the identification number in Tycho-2 Catalogue for the stars in common.

[3]Table 4.4 is available in electronic form at the CDS via anonymous ftp to cdsarc.u-strasbg.fr (130.79.128.5) or via `http://cdsweb.u-strasbg.fr/cgi-bin/qcat?J/A+A/381/464/`

4.2.1.1 Effectiveness of membership determination

Following Section 2.3.1.1, we obtained an effectiveness of membership determination of 0.77 for NGC 2548. This value, compared with the values of previous results for NGC 1817 (Sections 2.6.1.1 and 2.6.2.1), indicates that NGC 2548 shows, in the kinematical plane, a higher contrast over the field than NGC 1817.

4.2.2 The non-parametric approach

To complement the cluster/field segregation analysis of the astrometry from the previous section we have applied the non-parametric method to the proper motion data, as explained in Section 2.6.2. The details of the PDF calculation are explained in Section 2.6.2. The procedure was tested for several subsamples applying different proper motion cutoffs, and again satisfactory results are obtained for $|\mu| \leq 15$ mas yr^{-1}.

To resolve the empirical frequency functions we analised the areas of the VPD for the field and cluster and tested with circles of very different radii (see Figure 4.5 and Table 4.5), searching for the appropriate balance between cleanness and signal-to-noise ratio. The grid with cell size of 0.2 mas yr^{-1}, well below the proper motion errors, was used by the kernel density estimator in the VPD.

A clean frequency function with low cluster contamination and low noise was found in the area outside a circle with a radius of 35′ centred on the cluster. Figure 4.6 displays the empirical normalised frequency functions (PDFs) for the mixed population (circle), for the field (outside the circle) and for the cluster (non-field) population.

The typical noise level, γ, is evaluated from the negative density values found in some regions. As in Section 2.6.2, to avoid meaningless probabilities in zones of low density, we restricted the probability calculations to the stars with cluster PDF $\geq 3\gamma$. The maximum of the cluster PDF is located at $(\mu_\alpha \cos\delta, \mu_\delta) = (-1.2\pm0.2, 2.2\pm0.2)$ mas yr^{-1}.

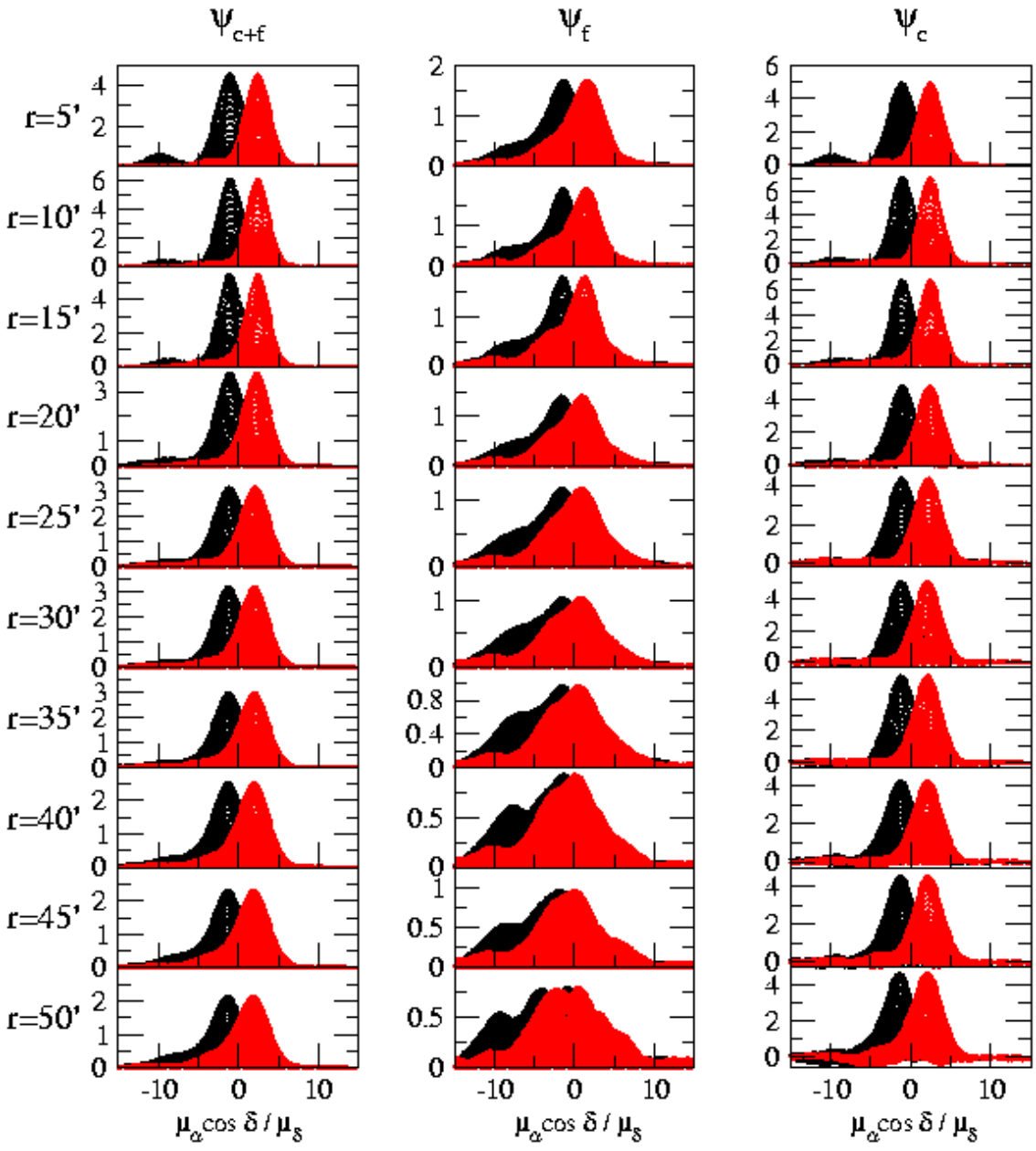

Figure 4.5: Empirical probability density functions for the mixed sample, ψ_{c+f}, the field population, ψ_f, and the cluster population, ψ_c, for NGC 2548 taking different radii, r At the back $\mu_\alpha \cos\delta$ in black, at the front μ_δ in red.

Table 4.5: Comparison of the position, maximum and FWHM of the empirical probability density function of the total, the field and the substracted cluster NGC 2548 taking different radii for the cluster area. The last column gives the FWHM for each component $(\mu_\alpha \cos\delta, \mu_\delta)$ and the averaged value.

r	$(\mu_\alpha \cos\delta)_{\rm c+f}$	$(\mu_\delta)_{\rm c+f}$	$(\psi_{\rm c+f})_{\rm max}$	$\mathrm{FWHM}_{\psi_{\rm c+f}}$
	$(\mu_\alpha \cos\delta)_{\rm f}$	$(\mu_\delta)_{\rm f}$	$(\psi_{\rm f})_{\rm max}$	$\mathrm{FWHM}_{\psi_{\rm f}}$
	$(\mu_\alpha \cos\delta)_{\rm c}$	$(\mu_\delta)_{\rm c}$	$(\psi_{\rm c})_{\rm max}$	$\mathrm{FWHM}_{\psi_{\rm c}}$
(arcmin)	(mas yr^{-1})	(mas yr^{-1})	-	(mas yr^{-1})
5	-1.0±0.2	2.4±0.2	4.6	4.0/3.6→3.8
	-1.4±0.2	1.6±0.2	1.7	5.0/5.2→5.1
	-1.0±0.2	2.4±0.2	4.9	4.0/4.8→4.4
10	-1.0±0.2	2.4±0.2	6.1	3.6/4.8→4.2
	-1.4±0.2	1.6±0.2	1.9	4.2/4.6→4.4
	-1.0±0.2	2.4±0.2	7.0	3.4/3.0→3.2
15	-1.0±0.2	2.4±0.2	5.5	3.4/4.8→4.1
	-1.4±0.2	1.2±0.2	1.8	4.4/4.4→4.4
	-1.0±0.2	2.4±0.2	6.8	3.2/3.0→3.1
20	-1.0±0.2	2.2±0.2	3.7	4.0/4.6→4.3
	-1.6±0.2	1.0±0.2	1.4	5.6/6.4→6.0
	-1.0±0.2	2.4±0.2	4.8	4.0/4.8→4.4
25	-1.2±0.2	2.2±0.2	3.2	4.4/4.2→4.3
	-1.6±0.2	1.0±0.2	1.2	7.0/7.2→7.1
	-1.2±0.2	2.2±0.2	4.4	4.2/4.4→4.3
30	-1.2±0.2	2.0±0.2	3.2	4.4/4.2→4.3
	-1.4±0.2	0.8±0.2	1.0	9.4/8.0→8.7
	-1.2±0.2	2.2±0.2	5.1	4.0/4.2→4.1
35	-1.2±0.2	2.0±0.2	3.0	4.4/4.2→4.3
	-1.4±0.2	0.6±0.2	1.0	10.2/8.6→9.4
	-1.2±0.2	2.2±0.2	5.5	4.2/4.2→4.2
40	-1.2±0.2	2.0±0.2	2.5	4.4/4.4→4.4
	-1.4±0.2	0.2±0.2	0.9	11.0/8.8→9.9
	-1.2±0.2	2.2±0.2	4.3	4.2/4.2→4.2
45	-1.2±0.2	2.0±0.2	2.3	4.4/4.6→4.5
	-1.8±0.2	0.0±0.2	1.0	11.0/8.2→9.6
	-1.2±0.2	2.2±0.2	4.6	4.2/4.2→4.2

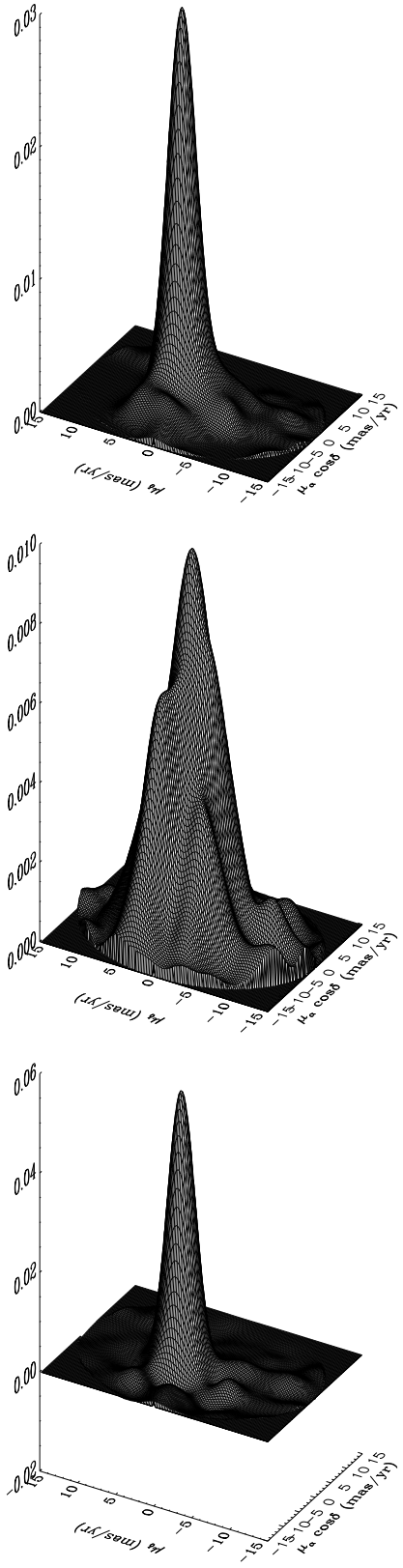

Figure 4.6: Empirical probability density functions in the kinematic plane. Top: ψ_{c+f} mixed sample from the inner circle of 35'. Centre: ψ_f field population from outside this circle. Bottom: ψ_c cluster population of NGC 2548

4.2.2.1 Effectiveness of membership determination

We also calculate the effectiveness of membership determination for the non-parametric approach. For NGC 2548 we found a value of $E = 0.67$. Not as high as in the parametric method, it stills points towards a noticeable contrast between cluster and field, making easier a proper segregation of cluster members.

4.2.3 The non-parametric approach in the spatial plane

As in Section 2.6.3 we check the spatial distribution of the cluster area, to try to use it to discriminate membership. We apply the kernel density estimator outside a circle of radius $35'$ to estimate the field frequency function. To extrapolate this frequency function to the inner circle we fitted a tilted plane to this distribution.

The mixed population PDF, ψ^s_{c+f}, is shown in Figure 4.7. For extended clusters with low contrast with the field, as happened also with NGC 1817, the spatial distribution shows not to be very discriminant for cluster/field segregation. Therefore, as well as in the classical approach the spatial distribution is not being considered in the segregation of cluster members in the NGC 2548.

4.2.4 Results and discussion

The cluster proper motion found with the non-parametric approach is different to the mean value found in Section 4.2.1. As discussed by many authors (Galadí-Enríquez et al. 1998a for instance) one of the limitations of the parametric approach is the trend of the circular Gaussian distribution, used to fit the cluster, to assume an excessive width to improve the representation of the field distribution. The cluster mean proper motion will then be thus affected. To measure the influence of this effect, we decided to apply the parametric method but to fix the internal velocity dispersion of the cluster to zero. This way the model will assign to the cluster Gaussian distribution a width related only to measurement errors. We obtained the distribution parameters and corresponding uncertainties shown in Table 4.6. We then obtained a mean proper motion of $(\mu_\alpha \cos\delta, \mu_\delta) = (-1.10\pm0.08, 2.09\pm0.08)$ mas yr^{-1}, in agreement with the cluster proper motion obtained by the non-parametric approach.

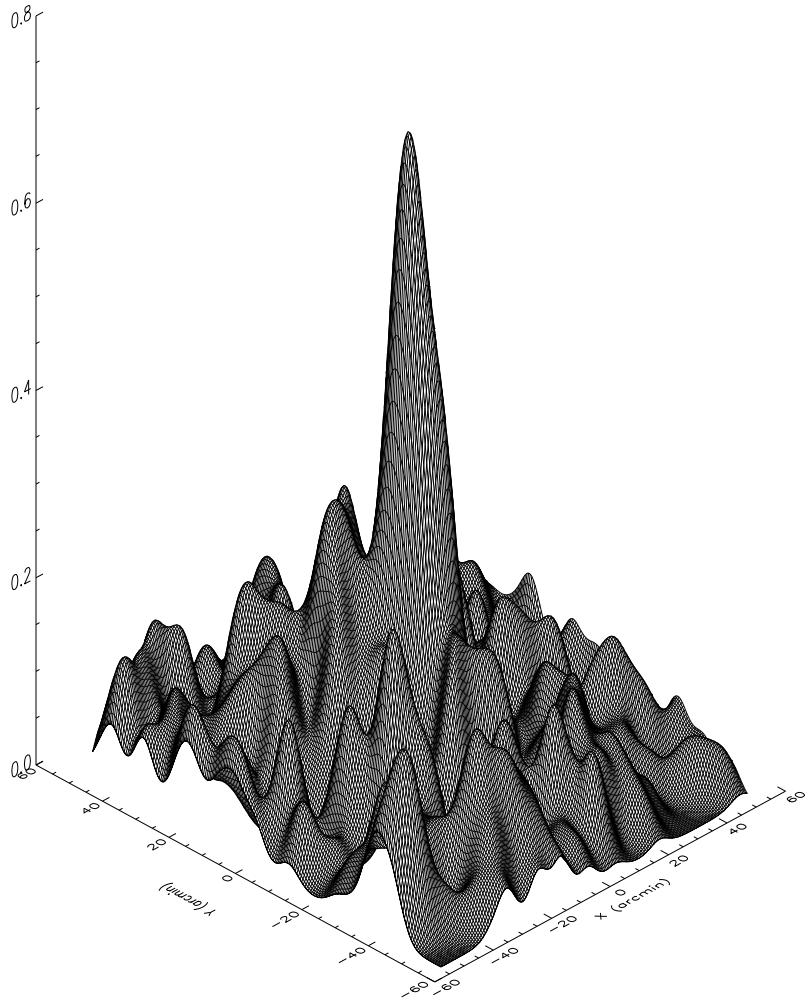

Figure 4.7: The empirical probability density function ψ^s_{c+f} in the spatial plane of NGC 2548.

Table 4.6: Distribution parameters and their uncertainties for NGC 2548 cluster and the field when $\sigma_c = 0$ is assumed. The units of μ and σ are mas yr^{-1}

	n_c	$\mu_\alpha \cos\delta$	μ_δ	$\sigma_{\mu_\alpha \cos\delta}$	σ_{μ_δ}	ρ
NGC 2548	0.188	−1.10	2.09			
	±0.021	±0.08	±0.08			
field		−4.13	−0.96	7.32	7.32	−0.26
		±0.09	±0.47	±0.04	±0.24	±0.03

As already mentioned in Section 2.6.4, the non-parametric technique does not take into account the errors of the individual proper motions, therefore it does not make any particular distinction between bright or faint stars, different epoch spread and so on. However, from the FWHM of the empirical cluster PDF an estimation of the errors of the distribution can be obtained. An FWHM of ∼4.2±0.2 mas yr^{-1} was obtained. Taking into account the Gaussian dispersion owing to the smoothing parameter h =1.44 mas yr^{-1}, this FWHM corresponds to a value of 1.53 mas yr^{-1}. But from Section 4.1, we know that the mean proper motion precision is 1.18 mas yr^{-1} which gives us an intrinsic dispersion component of 0.97 mas yr^{-1}, (3 km s^{-1} at the distance of 725 pc from Chapter 5), of the same order but slightly lower than the value obtained by the membership determination in Section 4.2.1. This indicates that the intrinsic velocity dispersion of the cluster cannot be neglected. Although fixing it to zero improves the determination of the mean motion of the cluster (position of the centre of the fitted Gaussian), the membership probability results are more meaningful taking into account the intrinsic dispersion. In our analysis of the parametric approach, we will use the parametric results from Section 4.2.1. Slight differences in the centre of the adopted Gaussian do not affect much the segregation, since the stars with highest probability of being members are almost the same in both cases.

A distinct separation between cluster members and field stars, in both approaches, can be seen in the cluster membership probability histogram in Figure 4.8. Solid line is the traditional parametric method from Section 4.2.1, dotted line is the non-parametric approach from Section 4.2.2. The integrated volume of the cluster frequency function in the non-parametric method gives us an expected number of 91 cluster members. In order of decreasing membership probability, P_{NP}, the first

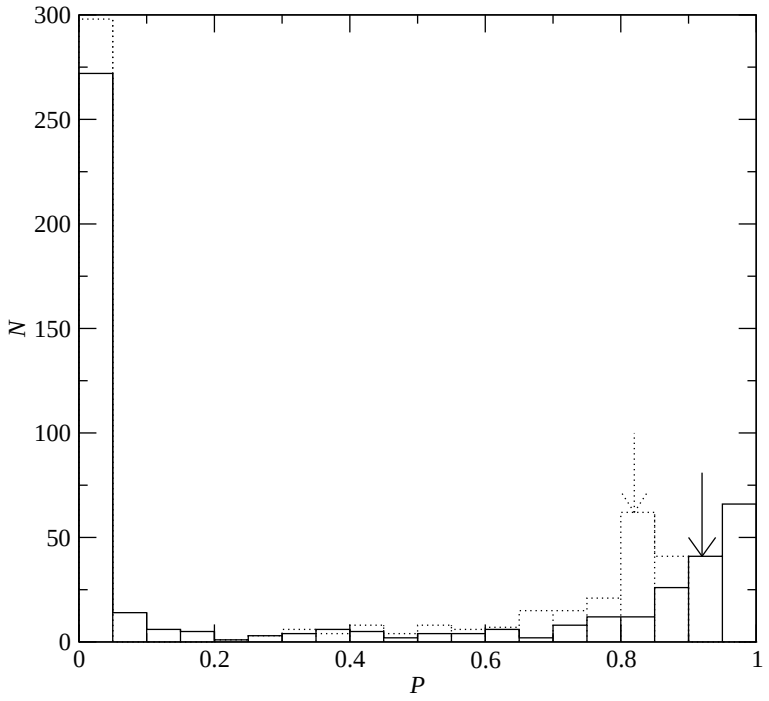

Figure 4.8: The histogram of cluster membership probability of NGC 2548. The solid line gives the results for traditional parametric method (Section 4.2.1), while the dotted line corresponds to the non-parametric approach (Section 4.2.2). The arrows mark the limiting probabilities for member selection for each method.

91 stars are the most probable cluster members. The minimum value of the non-parametric probability for the 91-st star is $P_{NP} = 0.82$. Table 4.7[4] lists the P_{NP} for the 501 stars.

There is no an equivalent rigorous way to decide where to set the limit among members and non-members in the list sorted in order of decreasing parametric membership probability, P_P. But, if we accept the size of the cluster predicted by the non-parametric method, 91 stars, we can consider that the 91 stars of highest P_P are the most probable members, according to the results of the parametric technique. The minimum value of the parametric probability (for the 91-st star) is $P_P = 0.92$.

With these limiting probabilities ($P_{NP} \geq 0.82$; $P_P \geq 0.92$), we get a 91% (458 stars) agreement in the segregation yielded by the two methods. The 43 remaining stars (9%) with contradicting segregation should be carefully studied. Discrepancies among the two approaches are actually expected due to the statistical nature of the methods themselves.

As in Chapter 2, to set up a final and unique list, and trying not to reject true members, we accept as probable members of this cluster those stars classified as members by at least one of the two methods. This way we get a list of 118 probable member stars.

Figures 4.9 and 4.10 show the final proper motion VPD and the sky distribution for all the measured stars, where "$\circ$" denotes a member star of NGC 2548, and all other stars are considered field stars indicated by "+".

Radial velocities have been studied by Geyer & Nelles (1985) with a focal reduced spectrograph. They give data for 23 stars but with a very low quality. The only accurate measurement is from Wallerstein et al. (1963) of star BDA 1560. Therefore, the available information on radial velocities is neither accurate nor complete enough to be useful in improving the membership segregation.

The cross-identification of our 8 stars in common with the Hipparcos Catalogue (ESA 1997) is shown in Table 4.8. Comparison with the membership determination calculated by Baumgardt et al. (2000) for the seven stars in common shows unequal agreement. Their mean astrometric parameters $(\mu_\alpha \cos\delta, \mu_\delta) =$

[4]Table 4.7 is available in electronic form at the CDS via anonymous ftp to cdsarc.u-strasbg.fr (130.79.128.5) or via `http://cdsweb.u-strasbg.fr/cgi-bin/qcat?J/A+A/437/457/`

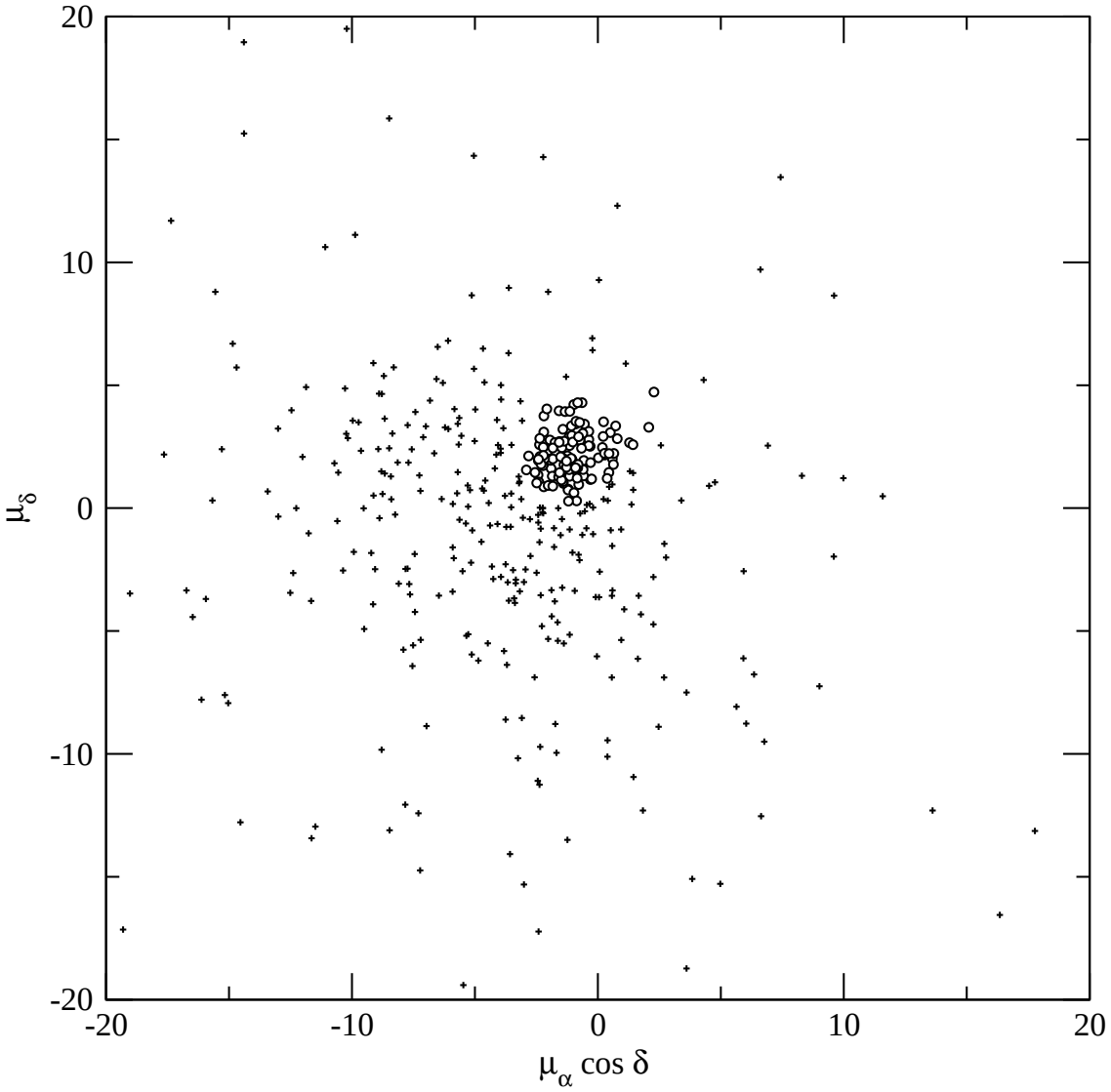

Figure 4.9: The proper motion vector-point diagram of stars in NGC 2548 region. (Units are mas yr^{-1}). "$\circ$" denotes a member star of NGC 2548 and "$+$" a field star.

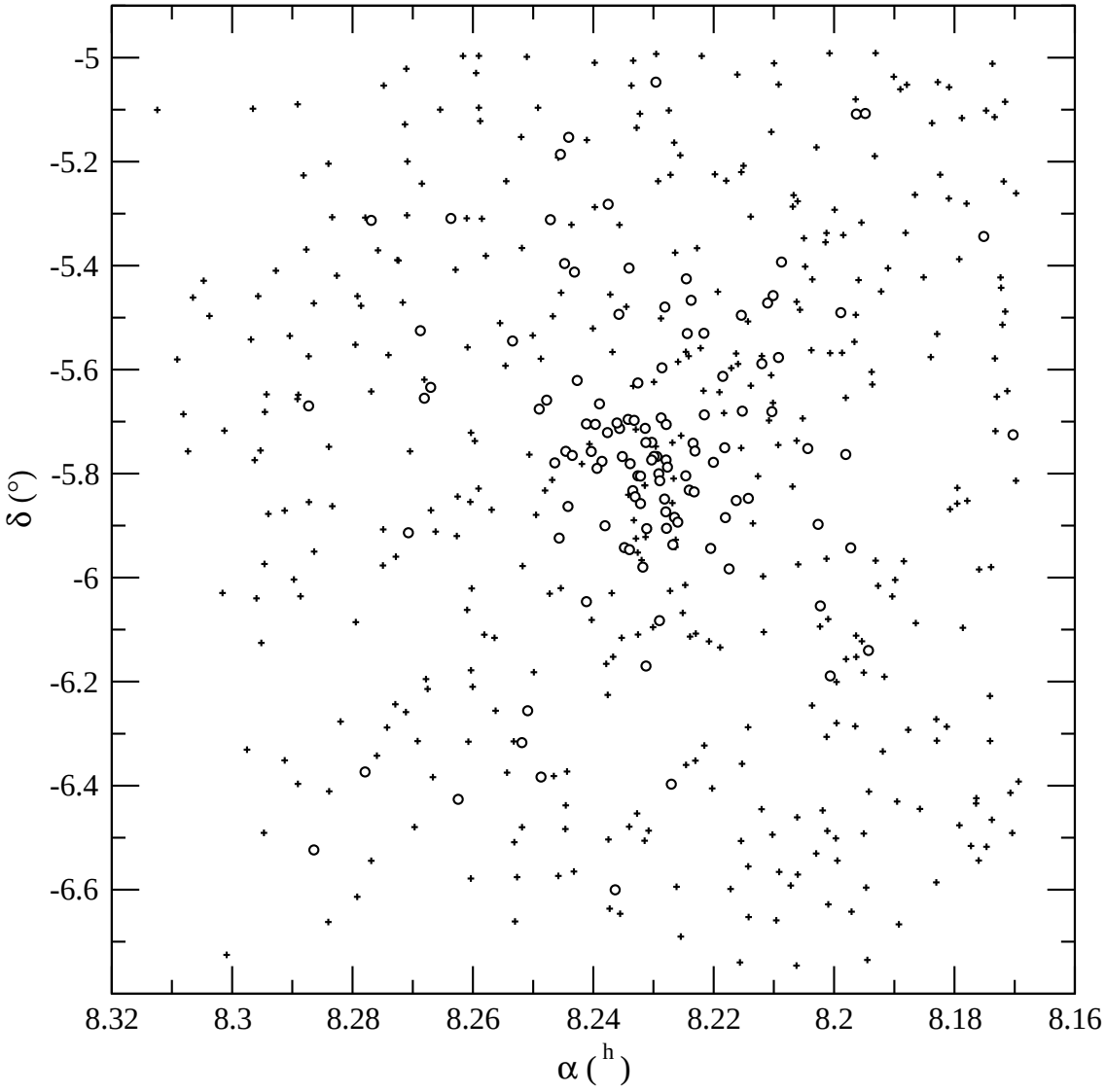

Figure 4.10: The position distribution of stars in NGC 2548 region. ("○" denotes a member star of NGC 2548 and "+" a field star)

Table 4.8: The cross-identification of stars in common with the Hipparcos Catalogue (ESA 1997) and the membership determination by Baumgardt et al. (2000). Comparison with our results P_P, P_{NP} and P_C is analysed in the text.

Table 4.4	Hipparcos	Tycho-2	BDA	Baumgardt et al. (2000)		This work		
				P	Member	P_P	P_{NP}	P_C
257	40110	4859_00078_1	366	0.0	NM	0.00	0.00	NM
140	40238	4859_00250_1	1005	86.3	M	0.87	0.67	NM
139	40254	4859_00036_1	1073	50.0	M	0.77	0.58	NM
133	40302	4855_01706_1	1320	82.0	M	0.78	0.59	NM
234	40348	4859_01156_1	1560	23.7	M	0.88	0.84	M
162	40362	4859_00092_1	1628	12.1	M	0.84	0.88	M
42	40498	4856_00072_1	2184	0.0	NM	0.00	0.00	NM
336	40281	4859_00921_1		0.0	NM	0.00	0.00	NM

(-0.50 ± 0.70,0.93 ± 0.65) mas yr^{-1} based on five stars considered members, are not very accurate and the membership associated to each of the 9 Hipparcos stars is, that way, biased. Their membership criteria needed to be complemented with other criteria (photometry, spectroscopy...).

We have studied twenty stars in the area of the secondary clump on the tidal tail proposed by Bergond et al. (2001). Only three of them appear to be cluster members (see Figure 4.11). The rest are randomly distributed in the VPD. Moreover, the contour plot of members shown in Figure 4.12 does not evidence any reliable clump. Although our limiting magnitude for astrometry $B_{\rm inst}\approx 14$ is brighter than the $B_{\rm cut}\approx 14.8$ of Bergond et al. (2001), it looks like this clump is not real. Unfortunately, our photometry (see the following Chapter) does not cover the clump area. Deeper studies will be necessary to confirm the existence of this clump.

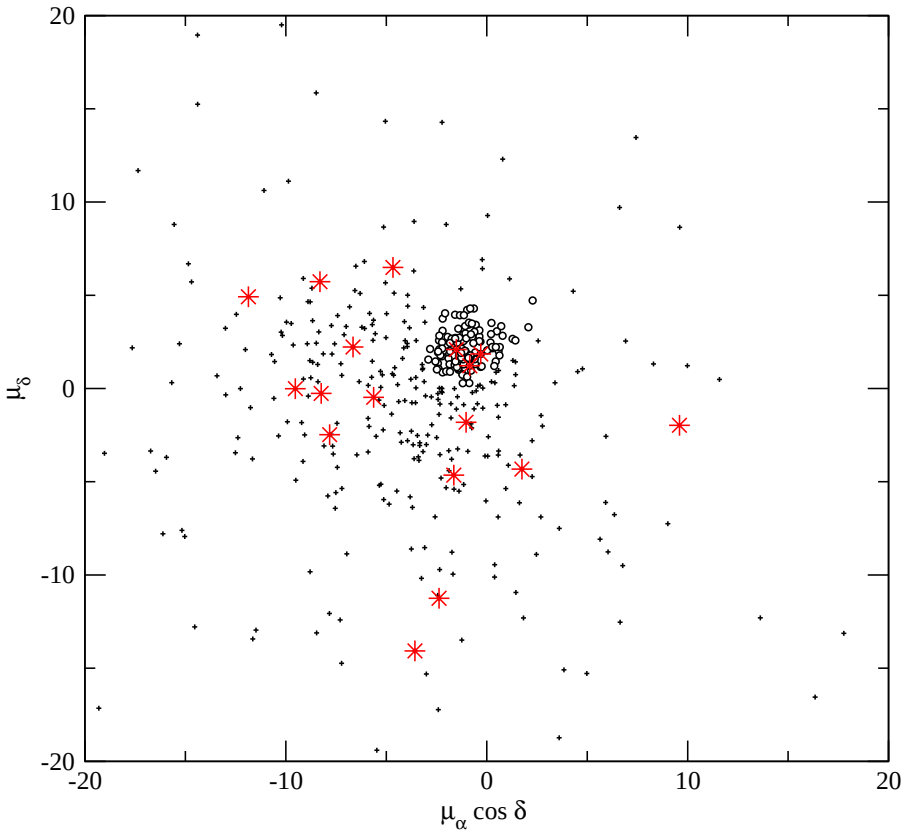

Figure 4.11: The proper motion vector-point diagram of stars in NGC 2548 region with the 20 stars located in the clump area marked as red big stars symbols. (Units are mas yr^{-1}).

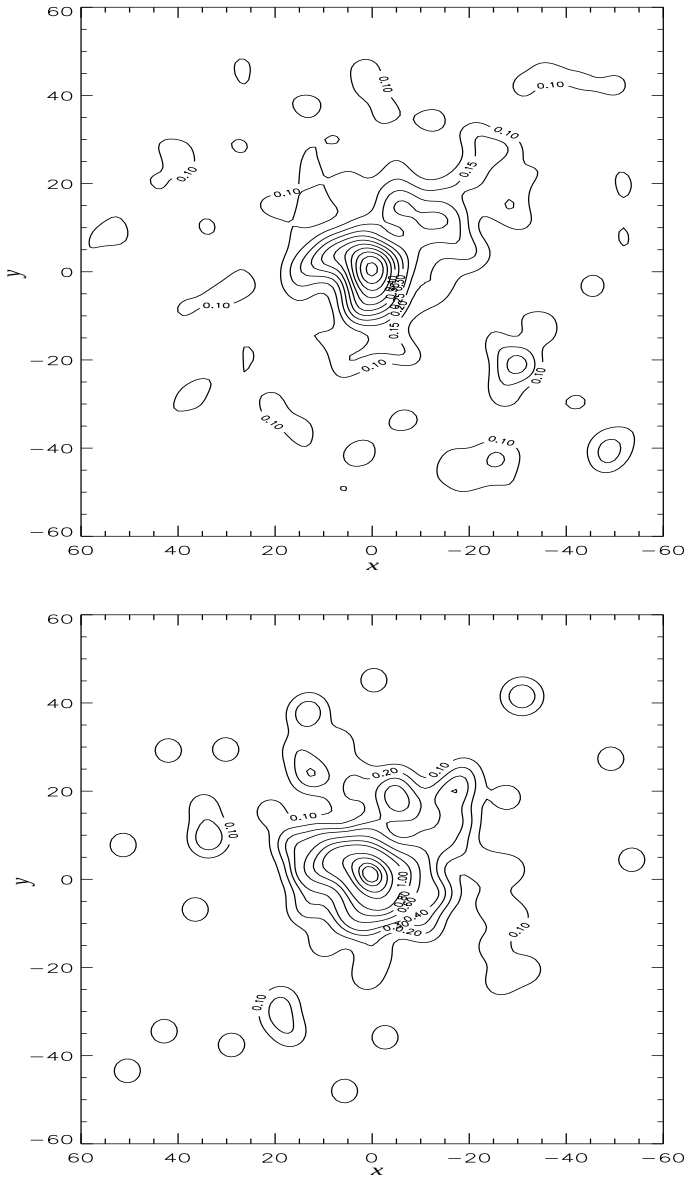

Figure 4.12: The contour plot of number counts of NGC 2548 area (upper plot) shows that the clump supposed to be at $(x, y) \sim (-30', -20')$ dissapears when we consider only members (lower plot). Units are arcmins. Axis (x, y) are orientated as (α, δ).